

耦合腔磁力系统中多透明窗口现象

廖庆洪*, 彭坤, 宋梦林

南昌大学信息工程学院电子信息工程系, 江西 南昌 330031

摘要 基于耦合腔磁力系统研究了多透明窗口现象以及快慢光效应。利用量子光学理论以及标准输入-输出关系, 对该系统的输出特性进行了研究。结果表明, 可以通过调节系统参数得到不同数目的透明窗口并得到较好的透明效果。同时, 提出了一种通过测量吸收峰高度和宽度来精密测量两腔之间的相互作用强度的方法。此外, 通过对系统参数进行调控, 可以实现快慢光转换。该方案在精密测量和量子信息处理等领域中具有重要的指导意义。

关键词 量子光学; 磁振子; 透明窗口; 腔磁力系统

中图分类号 O436 文献标志码 A

DOI: 10.3788/CJL230879

1 引言

随着纳米技术的高速发展, 腔光学已经成为一个重要的研究主题, 在量子光学领域中得到了广泛的关注^[1-6]。许多有趣的光学现象得到证实, 例如光力诱导透明^[7]、电磁诱导透明^[8]、机械振子的基态冷却^[9]、四波混频^[10]和双光子散射^[11]等。一个基本的腔光学系统模型由一面固定的镜子和一面可自由移动的镜子构成, 两面镜子通过辐射压耦合到腔场。近年来, 研究者将相关的研究推广到腔磁力系统中^[12]。腔磁力系统是具有腔场模式、磁振子模式和声子模式的复合系统, 磁振子通过磁光效应与光学腔场相互作用, 并通过磁致伸缩效应与机械振子相互作用^[13-15]。腔磁力系统具有良好的操控性、低损耗以及强耦合等优点, 是实现量子存储及量子信息处理的优良载体, 不仅可以作为研究量子信息学和量子光学的优秀平台, 还可以被用来探究宏观量子现象, 在量子信息处理、量子计算、量子精密测量和量子网络等诸多领域中有广泛的应用^[16-17]。研究者在腔磁力系统的背景下研究了许多有趣的现象, 如双稳态现象^[18]、磁力诱导透明、磁控制的慢光^[19]和非互易微波传输^[20]等。

磁振子是磁性材料中大量自旋的集体激发。钇铁石榴石(YIG)晶体是一种代表性的铁磁绝缘材料, 有丰富的磁非线性, 具有低耗散率和高自旋密度, 可以通过磁偶极相互作用实现磁振子和光子的强耦合^[21-22]。这为实现不同物理系统之间的信息传递提供了一个新平台。目前, 基于YIG小球的腔磁力系统已逐渐成为研究的热点。研究者在理论上提出了一种室温下的可

调慢光及其转化为快光的方法, 并实现了YIG小球中的自旋波量子 and 声子的耦合, 在自旋波量子与声子相互作用的基础上观察到了电磁诱导透明和吸收^[11]。Li等^[23]在由两个微波腔组成的腔磁力系统中, 利用双模压缩真空场驱动两个腔, 实现了声子-声子纠缠。湖南师范大学研究者在理论上研究了奇异点辅助的磁力诱导透明现象, 发现在奇异点附近, 探测光的传输出现抑制和恢复现象, 同时还实现了快慢光的调谐^[24]。侯宝成等^[25]研究了复合磁光力学系统中的相干光学传输特性。

基于文献[23-24], 本文提出了一种基于耦合腔磁力系统的多透明窗口的调谐方法。在实验上已经实现了YIG小球与三维微波腔的相互作用^[12]。此外, 两个腔之间通过能量交换进行耦合已经在实验中得到了实现, 且可以通过调节腔之间的距离来控制耦合强度的大小^[26]。因此, 基于YIG小球的耦合腔磁力系统在实验上是可行的。结果显示, 通过调节系统参数, 输出场的光学响应能得到有效的调控。这些特性在光开关、精密测量和量子信息处理等方面具有应用前景。

2 模型与理论

本文所研究的复合腔磁力系统如图1所示。其中两个YIG小球分别位于两个谐振腔的最大磁场附近, 并在两个谐振腔的 z 方向上对YIG小球施加偏置磁场以激发磁子模, 使其与腔场强耦合。磁致伸缩力会引起YIG球的振动, 从而产生声子模式。因此, 在YIG球中出现了磁振子-声子耦合^[12]。谐振腔 a_1 与谐振腔

收稿日期: 2023-05-31; 修回日期: 2023-06-17; 录用日期: 2023-07-04; 网络首发日期: 2023-08-07

基金项目: 国家自然科学基金(62061028)、南昌大学江西省财政科技专项“包干制”试点示范项目(ZBG20230418015)、上海市特殊人工微结构材料与技术重点实验室开放基金(ammt2021A-4)

通信作者: *nculqh@163.com

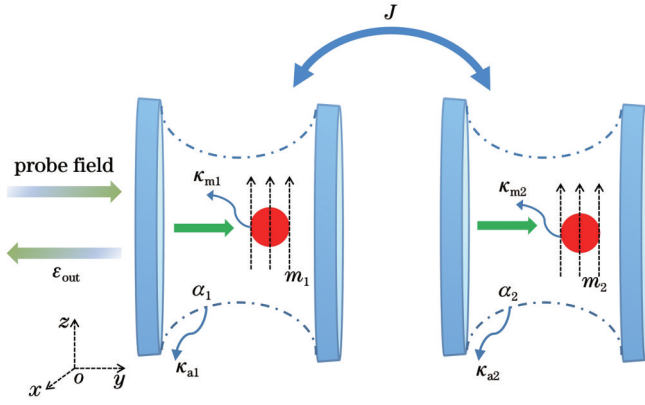


图 1 复合腔磁力系统示意图

Fig. 1 Schematic of hybrid cavity magnomechanical system

a_2 通过能量交换进行耦合, 耦合强度为 J 。在微波腔 a_1 的左侧施加一束较弱的探测光进行驱动, 其振幅为 $\epsilon_p = \sqrt{P_p / (\hbar \omega_p)}$, 其中, \hbar 为约化普朗克常数, ω_p 为频率, P_p 为探测场激光功率。

在驱动频率为 ω_0 的旋转框架下, 该系统的总哈密顿量为

$$\begin{aligned} H/\hbar = & \sum_{j=1,2} [\Delta_{a_j} a_j^\dagger a_j + \Delta_{m_j} m_j^\dagger m_j + \omega_b b_j^\dagger b_j + \\ & g_j (a_j^\dagger m_j + a_j m_j^\dagger) + G_{0j} m_j^\dagger m_j (b_j + b_j^\dagger) + \\ & i\Omega_j (m_j^\dagger - m_j)] + J (a_1^\dagger a_2 + a_1 a_2^\dagger) + \\ & i\epsilon_p [a_1^\dagger \exp(-i\delta t) - a_1 \exp(i\delta t)], \end{aligned} \quad (1)$$

式中: Δ_{a_j} 为腔场与泵浦场之间的失谐, $\Delta_{a_j} = \omega_{a_j} - \omega_0$; Δ_{m_j} 为磁振子与腔场之间的失谐, $\Delta_{m_j} = \omega_{m_j} - \omega_0$; δ 为探测场与泵浦场之间的失谐, $\delta = \omega_p - \omega_0$; a_j 、 m_j 和 b_j (a_j^\dagger 、 m_j^\dagger 和 b_j^\dagger) 分别是第 j 个腔模和磁振子及声子的湮灭 (产生) 算符, 且满足对易关系 $[o, o^\dagger] = 1 (o = a_j, m_j, b_j)$; ω_{a_j} 、 ω_{m_j} 和 ω_b 分别为谐振腔、磁振子和声子的共振频率; Ω_j 为真空拉比频率, $\Omega_j = \frac{\sqrt{5}}{4} \gamma \sqrt{N} B_0$, 其中, 幅值 $B_0 = 3.9 \times 10^{-9} \text{ T}$, 旋磁比 $\gamma = 28 \text{ GHz} \cdot \text{T}^{-1}$, 总自旋数 $N = \rho V$, YIG 小球的密度 $\rho = 4.22 \times 10^{27} \text{ m}^{-3}$, V 为 YIG 小球的体积; g_j 为腔光子-磁振子耦合强度; G_{0j} 为磁振子-声子耦合强度; t 为时间。式 (1) 中 $\Delta_{a_j} a_j^\dagger a_j$ 、 $\Delta_{m_j} m_j^\dagger m_j$ 、 $\omega_b b_j^\dagger b_j$ 分别表示谐振腔、磁振子和声子的自由哈密顿量; $g_j (a_j^\dagger m_j + a_j m_j^\dagger)$ 、 $G_{0j} m_j^\dagger m_j (b_j + b_j^\dagger)$ 、 $i\Omega_j (m_j^\dagger - m_j)$ 分别表示腔场-磁振子耦合哈密顿量、磁振子-声子耦合哈密顿量及驱动场与声子相互作用哈密顿量; $J (a_1^\dagger a_2 + a_1 a_2^\dagger)$ 、 $i\epsilon_p [a_1^\dagger \exp(-i\delta t) - a_1 \exp(i\delta t)]$ 为谐振腔之间相互作用哈密顿量及谐振腔 a_1 与探测场相互作用哈密顿量。

引入相应的耗散项和噪声项, 系统的海森堡-朗之

万动力学方程为

$$\begin{aligned} \dot{a}_1 = & -(i\Delta_{a_1} + \kappa_{a_1}) a_1 - ig_1 m_1 - iJa_2 + \\ & \epsilon_p \exp(-i\delta t) + \sqrt{2\kappa_{a_1}} a_1^{\text{in}}, \end{aligned} \quad (2)$$

$$\dot{a}_2 = -(i\Delta_{a_2} + \kappa_{a_2}) a_2 - ig_2 m_2 - iJa_1 + \sqrt{2\kappa_{a_2}} a_2^{\text{in}}, \quad (3)$$

$$\begin{aligned} \dot{m}_j = & -(i\Delta_{m_j} + \kappa_{m_j}) m_j - ig_j a_j - iG_{0j} m_j (b_j^\dagger + b_j) + \\ & \Omega_j + \sqrt{2\kappa_{m_j}} m_j^{\text{in}}, \end{aligned} \quad (4)$$

$$\dot{b}_j = -(i\omega_b + \gamma_j) b_j - iG_{0j} m_j^\dagger m_j + \sqrt{2\gamma_j} b_j^{\text{in}}, \quad (5)$$

式中: a_j^{in} 、 m_j^{in} 和 b_j^{in} 分别为谐振腔、磁振子和声子在系统中产生的具有零均值的阻尼以及噪声项, 可由非零相关函数 $\langle q^{\text{in}}(t) q^{\dagger(\text{in})}(t') \rangle = \delta(t - t')$ 表征, 其中, t' 为时间变量, $\delta(\cdot)$ 为狄拉克函数, $q = a_j, m_j, b_j$; κ_{a_j} 、 κ_{m_j} 和 γ_j 分别为谐振腔、磁振子和声子的耗散率。由于该复合腔磁力系统中探测场的强度远远小于驱动场的强度, 系统的量子力学性质可以采用线性化后的运动方程进行描述。将式 (2)~(5) 中的任意海森堡算符 (O) 表示为其稳态 (O_s) 与涨落项 (δO) 之和, 即 $O = O_s + \delta O (O = a_j, m_j, b_j)$ 。求得该系统的稳态解为

$$a_{1s} = -\frac{-i(g_1 m_1 + Ja_2)}{i\Delta_{a_1} + \kappa_{a_1}}, \quad (6)$$

$$a_{2s} = -\frac{-i(g_2 m_2 + Ja_1)}{i\Delta_{a_2} + \kappa_{a_2}}, \quad (7)$$

$$m_{js} = \frac{-ig_j a_j + \Omega_j}{i\Delta_j + \kappa_{m_j}}, \quad (8)$$

$$b_{js} = \frac{-iG_{0j} |m_{js}|^2}{i\omega_b + \gamma_j}, \quad (9)$$

式中: Δ_j 为谐振腔场与泵浦场之间的有效失谐, $\Delta_j = \Delta_{m_j} + G_{0j} (b_j^\dagger + b_j)$; K_j 为磁振子-声子的有效耦合强度, $K_j = G_{0j} m_{js}$ 。仅保留共振项的方程为

$$(i\lambda - \kappa_{a_1}) a_{1+} - ig_1 m_{1+} - iJa_{2+} + \epsilon_p = 0, \quad (10)$$

$$(i\lambda - \kappa_{a_2}) a_{2+} - ig_2 m_{2+} - iJa_{1+} = 0, \quad (11)$$

$$(i\lambda - \kappa_{m_j}) m_{j+} - ig_j a_{j+} - iK_j b_{j+} = 0, \quad (12)$$

$$(i\lambda - \gamma_j) b_{j+} - iK_j^* m_{j+} = 0, \quad (13)$$

式中: K_j^* 为 K_j 的共轭; m_{j+} 、 a_{j+} 和 b_{j+} 分别为 m_j 、 a_j 和 b_j 在频率 ω_p 处的响应; 在可分辨边带机制下令 $\lambda = \delta - \omega_b$, $\Delta_{a_j} = \Delta_j = \omega_b$ 。可得到输出场响应 a_{1+} 的表达式为

$$a_{1+} = \frac{\nu r_2 \epsilon_p}{r_1 r_2 - \xi_1 \xi_2}, \quad (14)$$

式中: $\nu = |K_1|^2 - (i\lambda - \kappa_{m_1})(i\lambda - \gamma_1)$; $r_j = (i\lambda - \kappa_{m_j}) \times (i\lambda - \gamma_j)(i\lambda - \kappa_{a_j}) + g_j^2 (i\lambda - \gamma_j) - (i\lambda - \kappa_{a_j}) |K_j|^2$; $\xi_j = iJ (i\lambda - \kappa_{m_j})(i\lambda - \gamma_j) - iJ |K_j|^2$ 。由标准输入-输出关系, 可得系统的输出场表达式, 即

$$\epsilon_{\text{out}} = \frac{2\kappa_{a_1} a_{1+}}{\epsilon_p}, \quad (15)$$

式中: ϵ_{out} 的实(虚)部为吸收(色散)。

3 数值结果与讨论

为了探究复合腔磁力系统的光学传输特性,本文采用的腔磁力系统实验参数^[10]为: $\omega_{a_1}/(2\pi) = \omega_{a_2}/(2\pi) = 10$ GHz, $\omega_{b_1}/(2\pi) = \omega_{b_2}/(2\pi) = 10$ MHz, $\kappa_{a_1}/(2\pi) = \kappa_{a_2}/(2\pi) = 2$ MHz, $J = 2\kappa_{a_1}$, $\kappa_{b_1}/(2\pi) = \kappa_{b_2}/(2\pi) = 100$ Hz, $g_1/(2\pi) = g_2/(2\pi) = 1.5$ MHz, $\kappa_{m_1}/(2\pi) = \kappa_{m_2}/(2\pi) = 0.1$ MHz, $K_1/(2\pi) = K_2/(2\pi) = 1.0$ MHz。

3.1 复合腔磁力系统中的多透明窗口现象

首先,探究不同耦合对本文所提出的复合腔磁力系统的作用,从而研究多透明窗口产生的物理原理。在图 2 中绘制了不同耦合强度下输出吸收光谱中的响应。在图 2(a)中,假设不含有两个微波腔之间的耦合强度及其与磁子和声子的耦合,仅含有腔 a_1 与磁子 m_1 之间的腔磁耦合。此时吸收谱出现一个磁诱导透明窗口,它是磁振子通过磁光效应与光学腔场相互作用产生的。当引入磁子与声子耦合时, $K_1 \neq 0$ 。此时,由于磁致伸缩效应,单个透明窗口分裂成两个透明窗口,如图 2(b)所示。两个透明窗口分别为磁诱导透明窗口及由磁子与声子相互作用产生的磁力诱导透明窗

口。进一步,打开两个谐振腔之间的耦合($J = 2\kappa_{a_1}$)。如图 2(c)所示,吸收谱出现的三个透明窗口,分别为磁诱导透明窗口、磁力诱导透明窗口和谐振腔之间相互作用产生的透明窗口。随后依次加入谐振腔 a_2 与磁子 m_2 之间的腔磁耦合,可以在图 2(d)中观察到双磁诱导透明现象。最后,考虑到所有耦合均不为 0,吸收谱中透明窗口分裂成 5 个窗口,其中包括 6 个波峰和 5 个波谷,如图 2(e)所示。此时,三个透明窗口分别为谐振腔之间相互作用产生的透明窗口、两个磁子与谐振腔之间相互作用产生的磁诱导透明窗口及两个磁子与声子相互作用产生的磁力诱导透明窗口。当谐振腔之间的耦合强度较大时,如图 2(f)所示,透明窗口的宽度变宽。随后,在图 3 中,绘制了不同耦合强度下探测场色散光谱中的响应与探测场归一化频率的关系。当只存在谐振腔 a_1 与磁子 m_1 之间的腔磁耦合时,单个磁诱导透明的色散谱如图 3(a)所示。当引入磁子与声子相互作用时,磁诱导透明和磁力诱导透明所产生的色散谱如图 3(b)所示。进一步依次加入两个微波腔之间的相互作用及谐振腔 a_2 与磁子 m_2 之间的腔磁耦合,其色散谱分别如图 3(c)、(d)所示。当所有 5 种耦合均存在时,输出场的色散谱如图 3(e)所示。最后,增大谐振腔之间的耦合强度,可以从图 3(e)、(f)看出,透明窗口的宽度明显增大。

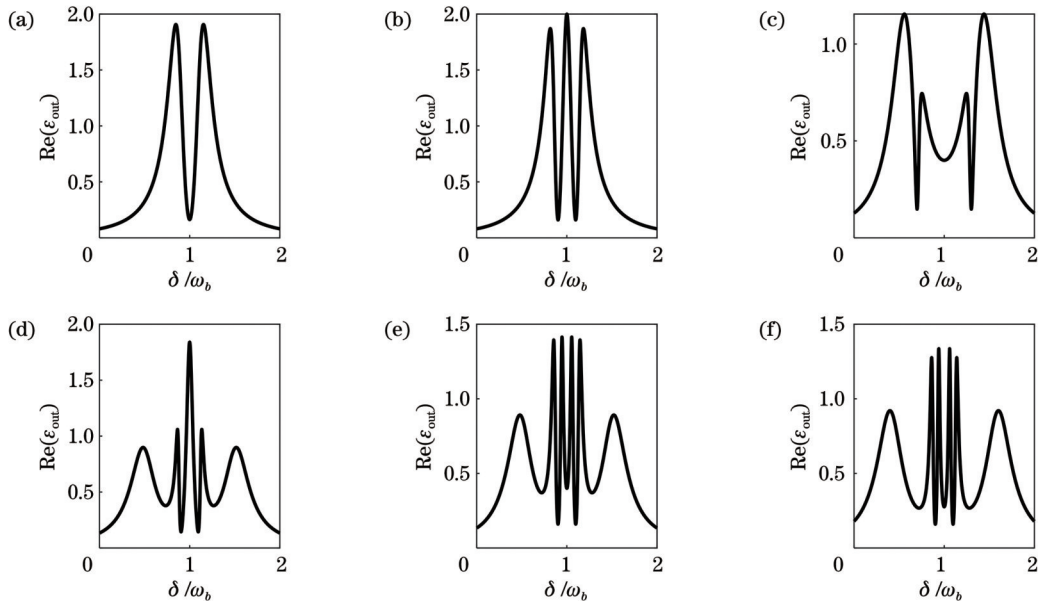


图 2 吸收谱 $\text{Re}(\epsilon_{\text{out}})$ 随归一化探测场失谐 δ/ω_b 的变化。(a) $g_1/(2\pi) = 1.5$ MHz, $g_2 = 0$, $K_1 = K_2 = 0$, $J = 0$; (b) $g_1/(2\pi) = 1.5$ MHz, $K_1/(2\pi) = 1.0$ MHz, $g_2 = 0$, $K_2 = 0$, $J = 0$; (c) $g_1/(2\pi) = 1.5$ MHz, $K_1/(2\pi) = 1.0$ MHz, $J = 2\kappa_{a_1}$, $g_2 = 0$, $K_2 = 0$; (d) $g_1/(2\pi) = g_2/(2\pi) = 1.5$ MHz, $K_1/(2\pi) = 1.0$ MHz, $J = 2\kappa_{a_1}$, $K_2 = 0$; (e) $g_1/(2\pi) = g_2/(2\pi) = 1.5$ MHz, $K_1/(2\pi) = K_2/(2\pi) = 1.0$ MHz, $J = 2\kappa_{a_1}$; (f) $g_1/(2\pi) = g_2/(2\pi) = 1.5$ MHz, $K_1/(2\pi) = K_2/(2\pi) = 1.0$ MHz, $J = 2.5\kappa_{a_1}$

Fig. 2 $\text{Re}(\epsilon_{\text{out}})$ versus δ/ω_b . (a) $g_1/(2\pi) = 1.5$ MHz, $g_2 = 0$, $K_1 = K_2 = 0$, $J = 0$; (b) $g_1/(2\pi) = 1.5$ MHz, $K_1/(2\pi) = 1.0$ MHz, $g_2 = 0$, $K_2 = 0$, $J = 0$; (c) $g_1/(2\pi) = 1.5$ MHz, $K_1/(2\pi) = 1.0$ MHz, $J = 2\kappa_{a_1}$, $g_2 = 0$, $K_2 = 0$; (d) $g_1/(2\pi) = g_2/(2\pi) = 1.5$ MHz, $K_1/(2\pi) = 1.0$ MHz, $J = 2\kappa_{a_1}$, $K_2 = 0$; (e) $g_1/(2\pi) = g_2/(2\pi) = 1.5$ MHz, $K_1/(2\pi) = K_2/(2\pi) = 1.0$ MHz, $J = 2\kappa_{a_1}$; (f) $g_1/(2\pi) = g_2/(2\pi) = 1.5$ MHz, $K_1/(2\pi) = K_2/(2\pi) = 1.0$ MHz, $J = 2.5\kappa_{a_1}$

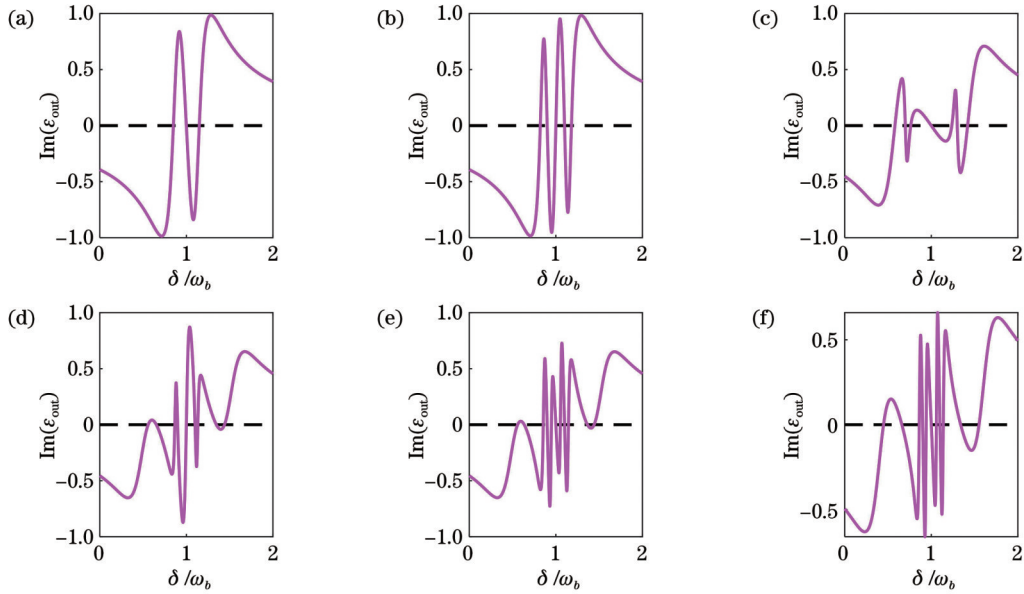


图 3 色散谱 $\text{Im}(\epsilon_{\text{out}})$ 随归一化探测场失谐 δ/ω_b 的变化。(a) $g_1/(2\pi) = 1.5 \text{ MHz}, g_2 = 0, K_1 = K_2 = 0, J = 0$; (b) $g_1/(2\pi) = 1.5 \text{ MHz}, K_1/(2\pi) = 1.0 \text{ MHz}, g_2 = 0, K_2 = 0, J = 0$; (c) $g_1/(2\pi) = 1.5 \text{ MHz}, K_1/(2\pi) = 1.0 \text{ MHz}, J = 2\kappa_{a_1}, g_2 = 0, K_2 = 0$; (d) $g_1/(2\pi) = g_2/(2\pi) = 1.5 \text{ MHz}, K_1/(2\pi) = 1.0 \text{ MHz}, J = 2\kappa_{a_1}, K_2 = 0$; (e) $g_1/(2\pi) = g_2/(2\pi) = 1.5 \text{ MHz}, K_1/(2\pi) = K_2/(2\pi) = 1.0 \text{ MHz}, J = 2\kappa_{a_1}$; (f) $g_1/(2\pi) = g_2/(2\pi) = 1.5 \text{ MHz}, K_1/(2\pi) = K_2/(2\pi) = 1.0 \text{ MHz}, J = 2.5\kappa_{a_1}$

Fig. 3 $\text{Im}(\epsilon_{\text{out}})$ versus δ/ω_b . (a) $g_1/(2\pi) = 1.5 \text{ MHz}, g_2 = 0, K_1 = K_2 = 0, J = 0$; (b) $g_1/(2\pi) = 1.5 \text{ MHz}, K_1/(2\pi) = 1.0 \text{ MHz}, g_2 = 0, K_2 = 0, J = 0$; (c) $g_1/(2\pi) = 1.5 \text{ MHz}, K_1/(2\pi) = 1.0 \text{ MHz}, J = 2\kappa_{a_1}, g_2 = 0, K_2 = 0$; (d) $g_1/(2\pi) = g_2/(2\pi) = 1.5 \text{ MHz}, K_1/(2\pi) = 1.0 \text{ MHz}, J = 2\kappa_{a_1}, K_2 = 0$; (e) $g_1/(2\pi) = g_2/(2\pi) = 1.5 \text{ MHz}, K_1/(2\pi) = K_2/(2\pi) = 1.0 \text{ MHz}, J = 2\kappa_{a_1}$; (f) $g_1/(2\pi) = g_2/(2\pi) = 1.5 \text{ MHz}, K_1/(2\pi) = K_2/(2\pi) = 1.0 \text{ MHz}, J = 2.5\kappa_{a_1}$

接下来,进一步研究两个微波腔之间的耦合强度对复合腔磁力系统传输特性的影响。如图 4 所示,绘制了不同耦合强度 J 下吸收曲线 $\text{Re}(\epsilon_{\text{out}})$ 随归一化探测场失谐 δ/ω_b 变化的曲线。可以看出,随着耦合强度 J 的增大,透明窗口的的位置没有发生改变,但是透明窗口的吸收峰峰值减小。此外,透明窗口的宽度随着 J 的增大发生了显著的变化。这一结果表明,通过调节耦合强度 J 的大小,在输出场能够得到更好的透明。为了进一步讨论 J 对探测场吸收光谱的影响,绘制了

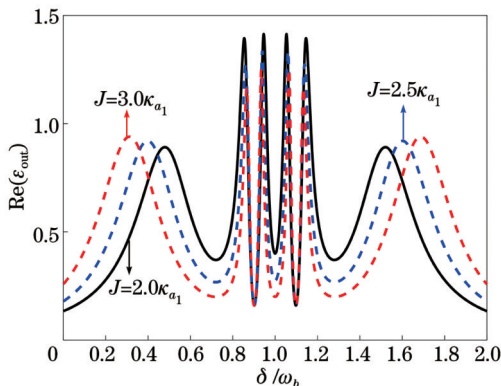


图 4 不同耦合强度下吸收谱 $\text{Re}(\epsilon_{\text{out}})$ 随归一化探测场失谐 δ/ω_b 的变化

Fig. 4 $\text{Re}(\epsilon_{\text{out}})$ versus δ/ω_b under different coupling strength values

探测场吸收光谱的吸收峰高度 (H) 和宽度 (W) 随耦合强度 J 变化的曲线,如图 5 所示。结果表明,探测场吸收光谱的吸收峰的高度与两个微波腔的耦合强度 J 成反比,宽度与 J 成正比。因此,可以通过简单测量吸收峰的高度和宽度,获得耦合强度 J 的大小。

如图 6 所示,当磁子与声子的耦合强度分别为 $K_1/(2\pi) = K_2/(2\pi) = 1.0 \text{ MHz}, K_1/(2\pi) = K_2/(2\pi) =$

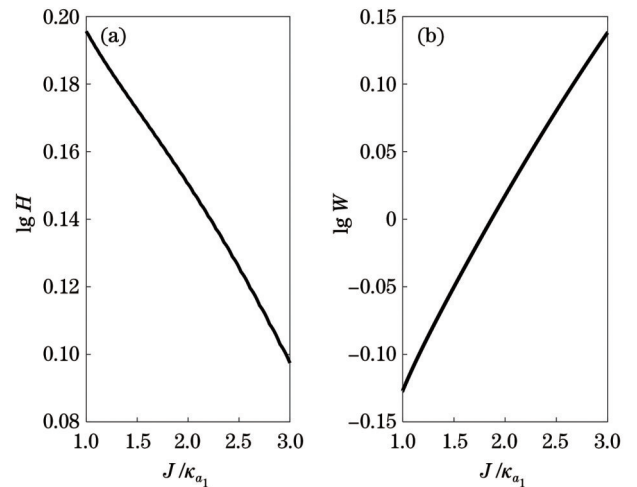


图 5 耦合强度对吸收峰的影响。(a) 吸收峰高度;(b) 吸收峰宽度

Fig. 5 Influence of coupling strength on absorption peak. (a) Absorption peak height; (b) absorption peak width

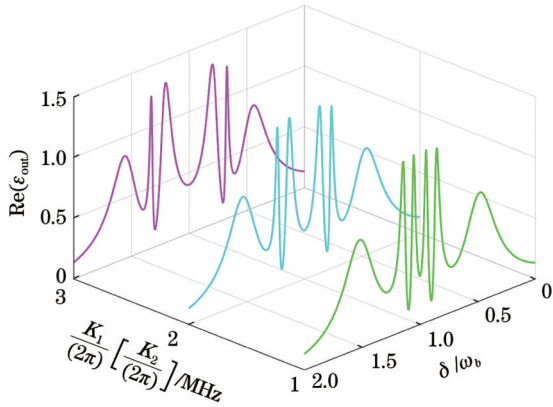


图6 不同磁子与声子耦合强度下 $\text{Re}(\epsilon_{\text{out}})$ 随 δ/ω_b 的变化
Fig. 6 $\text{Re}(\epsilon_{\text{out}})$ versus δ/ω_b under different magnon-phonon coupling strength values

2.0 MHz, $K_1/(2\pi) = K_2/(2\pi) = 3.0$ MHz 时, 绘制了探测场吸收光谱随归一化探测场失谐 δ/ω_b 的变化。

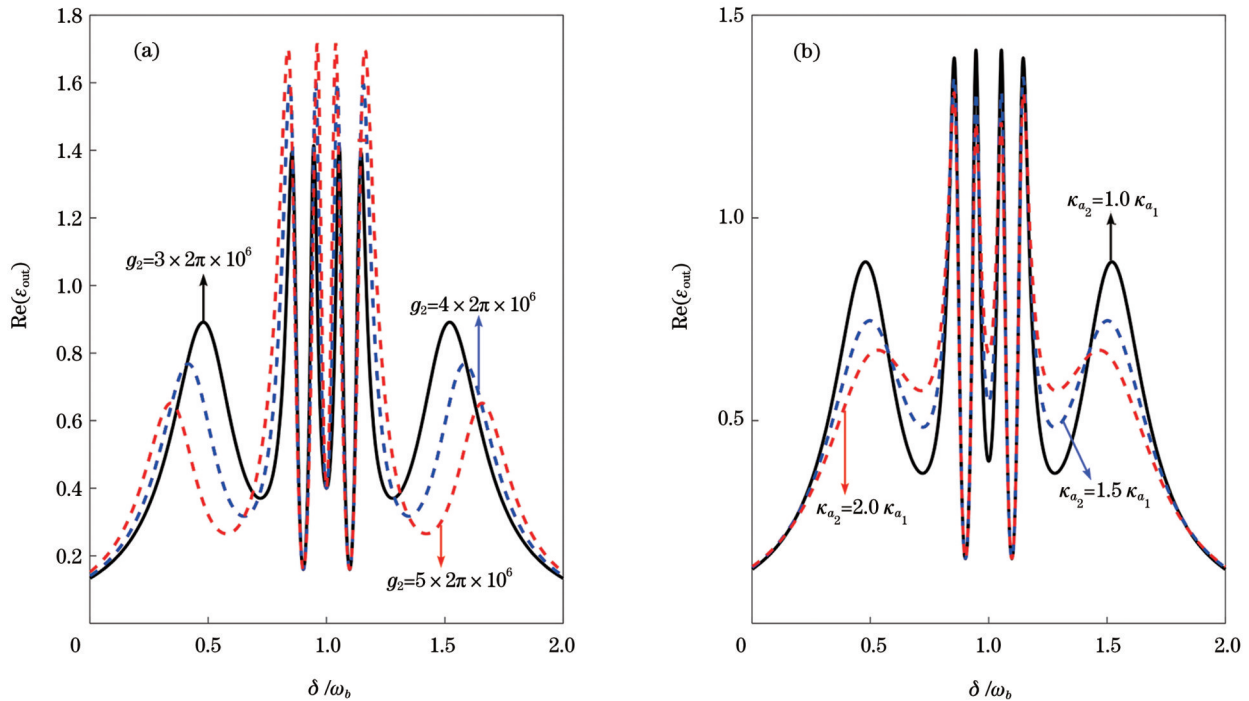


图7 g_2 和 κ_{a_2} 对探测场吸收光谱的影响。(a) 不同磁子与谐振腔耦合强度下 $\text{Re}(\epsilon_{\text{out}})$ 随归一化探测场失谐 δ/ω_b 的变化; (b) 不同谐振腔耗散下 $\text{Re}(\epsilon_{\text{out}})$ 随归一化探测场失谐 δ/ω_b 的变化

Fig. 7 Influence of g_2 and κ_{a_2} on absorption spectrum of detection field. (a) $\text{Re}(\epsilon_{\text{out}})$ versus δ/ω_b under different magnon-cavity coupling strength values; (b) $\text{Re}(\epsilon_{\text{out}})$ versus δ/ω_b under different resonator dissipation values

3.2 复合腔磁力系统中的群延迟效应

在 3.1 节中, 详细讨论了复合腔磁力系统中的多透明窗口现象。下面将进一步探讨复合腔磁力系统中的群延迟效应。群延迟表达式可定义为

$$\tau = \frac{d\phi(\omega_p)}{d\epsilon_{\text{out}}} = \text{Im} \left[\frac{1}{\epsilon_{\text{out}}} \times \frac{\partial \epsilon_{\text{out}}}{\partial \omega_b} \right], \quad (16)$$

式中: $\phi(\omega_p) = \arg[\epsilon_{\text{out}}(\omega_p)]$ 。在物理上, $\tau > 0$ ($\tau < 0$) 表示系统出现了慢光(快光)。

随着磁子与声子的耦合强度的增大, 位于共振处 $\delta = \omega_b$ 的透明窗口的宽度逐渐增大, 同时位于 $\delta = \omega_b$ 左右的两个透明窗口略有变宽。与图 5 类似, 可绘制位于 $\delta = \omega_b$ 处的透明窗口的宽度随磁子与声子耦合强度变化的曲线, 从而能够通过测量透明窗口的宽度对耦合强度实现精密测量。进一步, 探究了不同的腔 a_2 和磁子 m_2 之间的腔磁耦合强度 g_2 及谐振腔 a_2 的耗散 κ_{a_2} 对探测场吸收光谱的影响, 结果如图 7 所示。尽管参数 κ_{a_2} 和 g_2 的取值不同, 但是位于中间的两个透明窗口的间距并未发生改变。因为这三个透明窗口的间距与磁子和声子的耦合强度 K_1 和 K_2 有关, 而与其他参数无关。简而言之, 谐振腔 a_2 的耗散 κ_{a_2} 及腔 a_2 和磁子 m_2 之间的腔磁耦合强度 g_2 只会造成吸收光谱的吸收峰的位置发生改变, 而不会影响透明窗口的位置。可以通过选择合适的 g_2 、 κ_{a_2} 值得到更好的透明效果。

图 8 分别给出了在不同的谐振腔耗散 κ_{a_2} 与耦合强度 J 下, 群延迟 τ 随归一化探测场失谐 δ/ω_b 的变化。可以看出, 在 $\delta = 0.7\omega_b$ 与 $\delta = 1.3\omega_b$ 附近, 均存在向上的峰(慢光效应)和向下的谷(快光效应), 并且群延迟 τ 的峰值随腔的耗散的增大而减小, 随耦合强度的增大而增大。因此, 可以通过改变谐振腔的耗散以及耦合强度的大小实现快慢光效应之间的转换。

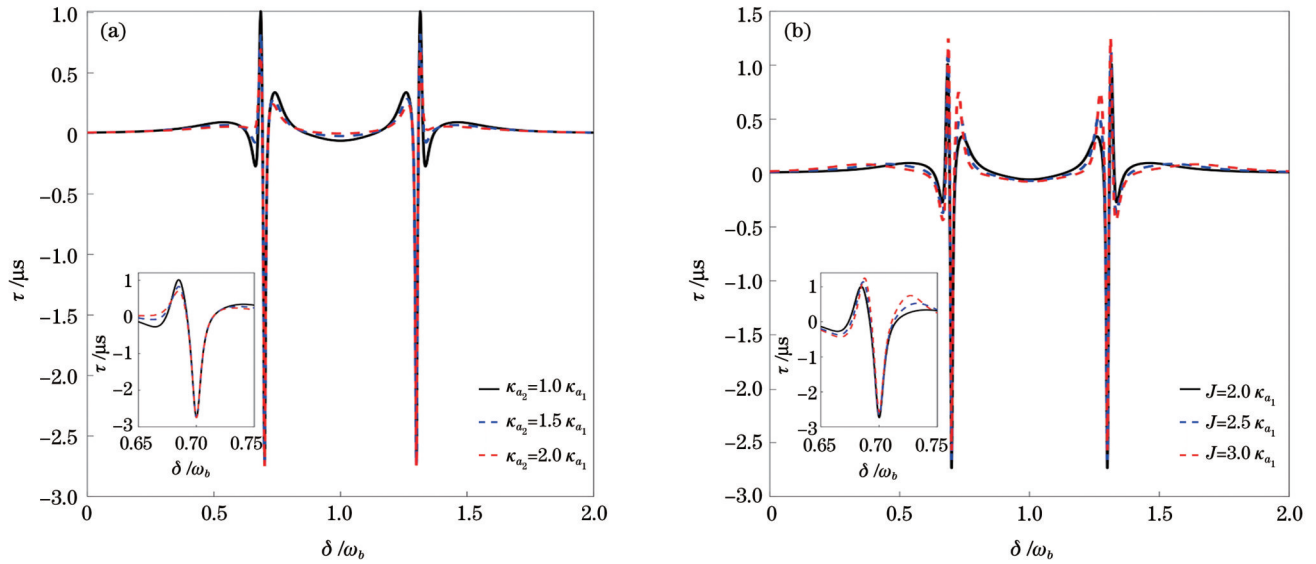


图 8 不同条件下 τ 随 δ/ω_b 的变化。(a) 不同谐振腔耗散; (b) 不同耦合强度

Fig. 8 τ versus δ/ω_b under different conditions. (a) Under different resonator dissipation values; (b) under coupling strength values

4 结 论

基于腔磁力系统的物理特性,研究了多透明窗口现象以及快慢光效应。首先,研究了系统中各耦合系数对输出场吸收光谱的影响。结果显示,可以通过合理选择耦合参数,得到不同数目的透明窗口,同时通过对系统参数进行调控,在输出探测场可得到较好的透明效果。其次,通过研究透明窗口宽度和高度与两腔之间耦合强度的关系,提出了一种通过测量吸收峰高度和宽度来精密测量两腔之间的相互作用强度的方法。此外,通过研究不同参数对快慢光效应的影响,实现快了慢光效应之间的转换。

参 考 文 献

- [1] Marquardt F, Chen J P, Clerk A A, et al. Quantum theory of cavity-assisted sideband cooling of mechanical motion[J]. *Physical Review Letters*, 2007, 99(9): 093902.
- [2] Andersson G, Ekström M K, Delsing P. Electromagnetically induced acoustic transparency with a superconducting circuit[J]. *Physical Review Letters*, 2020, 124(24): 240402.
- [3] Liao Q H, Xiao X, Nie W J, et al. Transparency and tunable slow-fast light in a hybrid cavity optomechanical system[J]. *Optics Express*, 2020, 28(4): 5288-5305.
- [4] 王婧. 基于三腔光力学系统的非互易性研究[J]. *激光与光电子学进展*, 2020, 57(19): 191201.
Wang J. Nonreciprocity in a three-cavity optomechanical system[J]. *Laser & Optoelectronics Progress*, 2020, 57(19): 191201.
- [5] Horodecki R, Horodecki P, Horodecki M, et al. Quantum entanglement[J]. *Reviews of Modern Physics*, 2009, 81(2): 865-942.
- [6] 李刚, 张鹏飞, 杨鹏飞, 等. 光学腔与原子强耦合的实验研究进展[J]. *光学学报*, 2022, 42(3): 0327005.
Li G, Zhang P F, Yang P F, et al. Experimental progress of strongly coupling between optical cavity and atoms[J]. *Acta Optica Sinica*, 2022, 42(3): 0327005.
- [7] Zheng M H, Wang T, Wang D Y, et al. Manipulation of multi-transparency windows and fast-slow light transitions in a hybrid cavity optomechanical system[J]. *Science China Physics, Mechanics & Astronomy*, 2019, 62(5): 950311.
- [8] Guo Y J, Li K, Nie W J, et al. Electromagnetically-induced-transparency-like ground-state cooling in a double-cavity optomechanical system[J]. *Physical Review A*, 2014, 90(5): 053841.
- [9] Lai D G, Huang J F, Yin X L, et al. Nonreciprocal ground-state cooling of multiple mechanical resonators[J]. *Physical Review A*, 2020, 102(1): 011502.
- [10] 廖庆洪, 邱海燕, 喻富, 等. 三腔复合光力系统的透射谱和四波混频现象研究[J]. *中国激光*, 2023, 50(14): 1412001.
Liao Q H, Qiu H Y, Yu F, et al. Transmission spectrum and four-wave mixing in a three-cavity optomechanical system[J]. *Chinese Journal of Lasers*, 2023, 50(14): 1412001.
- [11] 陈冬成, 周岳辉, 黄金凤, 等. 混合腔光力系统的双光子散射[J]. *光学学报*, 2022, 42(3): 0327015.
Chen D C, Zhou Y H, Huang J F, et al. Two-photon scattering in mixed cavity optomechanical system[J]. *Acta Optica Sinica*, 2022, 42(3): 0317015.
- [12] Zhang X F, Zou C L, Jiang L, et al. Cavity magnomechanics[J]. *Science Advances*, 2016, 2(3): e1501286.
- [13] Lachance-Quirion D, Tabuchi Y, Ishino S, et al. Resolving quanta of collective spin excitations in a millimeter-sized ferromagnet[J]. *Science Advances*, 2017, 3(7): e1603150.
- [14] Li J E, Zhu S Y, Agarwal G S. Magnon-photon-phonon entanglement in cavity magnomechanics[J]. *Physical Review Letters*, 2018, 121(20): 203601.
- [15] Harder M, Yao B M, Gui Y S, et al. Coherent and dissipative cavity magnonics[J]. *Journal of Applied Physics*, 2021, 129(20): 201101.
- [16] Yuan H Y, Cao Y S, Kamra A, et al. Quantum magnonics: when magnon spintronics meets quantum information science[J]. *Physics Reports*, 2022, 965: 1-74.
- [17] Wang K, Gao Y P, Jiao R Z, et al. Recent progress on optomagnetic coupling and optical manipulation based on cavity-optomagnonics[J]. *Frontiers of Physics*, 2022, 17(4): 042201.
- [18] Wang Y P, Zhang G Q, Zhang D K, et al. Bistability of cavity magnon polaritons[J]. *Physical Review Letters*, 2018, 120(5): 053601.

- 057202.
- [19] Ullah K, Naseem M T, Müstecaplıoğlu Ö E. Tunable multiwindow magnomechanically induced transparency, Fano resonances, and slow-to-fast light conversion[J]. *Physical Review A*, 2020, 102(3): 033721.
- [20] Wang Y P, Rao J W, Yang Y, et al. Nonreciprocity and unidirectional invisibility in cavity magnonics[J]. *Physical Review Letters*, 2019, 123(12): 127202.
- [21] Zhang X F, Zou C L, Jiang L A, et al. Strongly coupled magnons and cavity microwave photons[J]. *Physical Review Letters*, 2014, 113(15): 156401.
- [22] Goryachev M, Farr W G, Creedon D L, et al. High-cooperativity cavity QED with magnons at microwave frequencies[J]. *Physical Review Applied*, 2014, 2(5): 054002.
- [23] Li J E, Gröblacher S. Entangling the vibrational modes of two massive ferromagnetic spheres using cavity magnomechanics[J]. *Quantum Science and Technology*, 2021, 6(2): 024005.
- [24] Lu T X, Zhang H L, Zhang Q A, et al. Exceptional-point-engineered cavity magnomechanics[J]. *Physical Review A*, 2021, 103(6): 063708.
- [25] 侯宝成, 陈华俊. 辅助腔增强磁光力系统中的相干光学传输[J]. *中国激光*, 2023, 50(6): 0612001.
Hou B C, Chen H J. Coherent optical transmission in magneto-optomechanical systems enhanced by auxiliary cavity[J]. *Chinese Journal of Lasers*, 2023, 50(6): 0612001.
- [26] Peng B, Özdemir Ş K, Chen W J, et al. What is and what is not electromagnetically induced transparency in whispering-gallery microcavities[J]. *Nature Communications*, 2014, 5: 5082.

Multi-transparent Window Phenomenon in Coupled Cavity Magnomechanical System

Liao Qinghong*, Peng Kun, Song Menglin

Department of Electronic Information Engineering, School of Information Engineering, Nanchang University, Nanchang 330031, Jiangxi, China

Abstract

Objective With the rapid developments in nanotechnology, cavity optomechanics has become an important research topic in quantum mechanics. Magnomechanical cavity systems have attracted considerable attention in recent years. Compared to the cavity optomechanical system, the cavity magnomechanical system exhibits many benefits such as high spin density, high cooperativity with microwave photons, and a very low damping rate. Therefore, this study provides a new platform for examining interactions between light and matter. This study analyzes the multi-transparent window phenomenon, fast- and slow-light effects, and precision measurements in a coupled cavity magnomechanical system. These results have potential applications in quantum information processing and high-precision measurements.

Methods In this study, we commence with a coupled cavity magnomechanical system model. The hybrid cavity magnomechanical system consists of two yttrium iron garnet (YIG) balls located near the maximum magnetic field of the two resonant cavities, and a bias magnetic field is applied to the YIG balls in the z -direction of the two resonant cavities to excite the magnon mode and realize strong coupling with the cavity field. Mutual coupling exists between the optical fields of the two resonators, and the coupling strength is related to the distance between them. A weak probe laser beam ϵ_p with frequency ω_p is applied to the optical cavity a_1 . The total Hamiltonian of the coupled cavity-magnetic field can be obtained in a frame rotating at the frequency of the driving field. Based on the Heisenberg equation and input-output relationship, we can obtain the output field (ϵ_{out}) expression and group delay (τ) expression of the system. Subsequently, the effects of various parameters on the optical response of the system are investigated.

Results and Discussions When the coupling between two microwave cavities and magnon-phonon coupling are absent, there is only photon-magnon coupling between the cavity a_1 and magnon m_1 . At this time, there is a magnon-induced transparency window in the absorption spectrum generated by the interaction between the magnon and optical cavity field. We introduce various coupling terms, and the absorption spectrum of the output field exhibits different numbers of transparent windows (Fig. 2). The dispersion spectrum of the output field is plotted under the same conditions (Fig. 3). Next, the influence of the coupling strength between the two microwave cavities on the transmission characteristics of the hybrid cavity magnomechanical system is examined. These results indicate that better transparency can be realized in the output field by adjusting the coupling strength using the coupling strength (Fig. 4). The absorption peak heights and widths of the detection field absorption spectra are plotted as a function of the coupling strength (Fig. 5). The results indicate that the absorption peak height of the detection field absorption spectrum is inversely proportional to the coupling strength (J) of the two microwave cavities, and the width is directly proportional to J . Therefore, the coupling strength J can be obtained by simply measuring the height and width of the absorption peak, which also indicates that the hybrid cavity magnomechanical system is an effective and accurate method for measuring the coupling strength J . We also investigate

the effects of K_1 , K_2 , g_2 , and κ_{a_2} on the output field (Figs. 6 and 7). The results show that g_2 and κ_{a_2} only cause a change in the position of the absorption peak of the absorption spectrum and do not affect the position of the transparent window. Finally, the functions of the group delay (τ) with the normalized detection field detuning (δ/ω_b) are plotted for different J and κ_{a_2} (Fig. 6). There are upward peaks (slow-light effect) and downward valleys (fast-light effect) near $\delta = 0.7\omega_b$ and $\delta = 1.3\omega_b$, and the peak value of the group delay τ decreases with an increase in cavity dissipation κ_{a_2} and increases with an increase in coupling strength J . Therefore, the conversion between fast- and slow-light effects can be realized by changing the dissipation and coupling strengths of the resonant cavity.

Conclusions Based on the coupled cavity magnomechanical system, the phenomenon of multiple transparent windows and effect of slow-fast light are investigated. The output characteristics of the system are discussed using quantum optics theory and standard input-output relations. The results show that different numbers of transparent windows can be obtained by adjusting the system parameters, and better transparency can be realized. Simultaneously, a method for precisely measuring the interaction strength between the two cavities is proposed by measuring the height and width of the absorption peaks. Additionally, fast-slow light conversion can be achieved by adjusting the system parameters. This scheme has important guiding significance for research on precision measurements and quantum information processing.

Key words quantum optics; magnon; transparent window; cavity magnomechanical system